Graphical Abstract

3D lightweight mechanical metamaterial with nearly isotropic inelastic large deformation response

Xueyan Chen[a,b], Johnny Moughames[b], Qingxiang Ji[a,b], Julio Andrés Iglesias Martínez[b], Huifeng Tan[a], Gwenn Ulliac[b], Vincent Laude[b], Muamer Kadic[b]

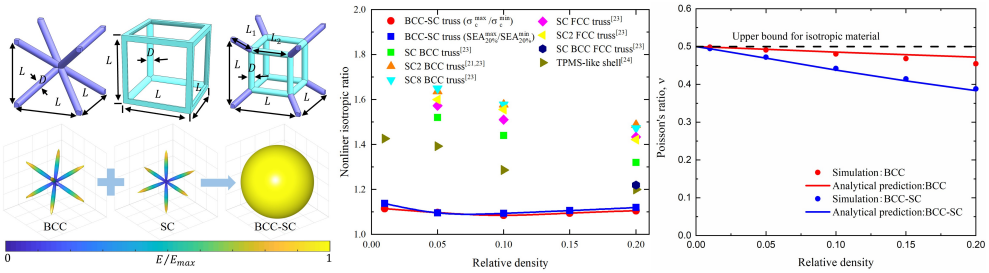

Highlights

3D lightweight mechanical metamaterial with nearly isotropic inelastic large deformation response

Xueyan Chen[a,b], Johnny Moughames[b], Qingxiang Ji[a,b], Julio Andrés Iglesias Martínez[b], Huifeng Tan[a], Gwenn Ulliac[b],Vincent Laude[b], Muamer Kadic[b]

- A class of isotropic bending dominated truss lattice materials with stable inelastic large response is introduced.
- A model successfully predicts elastic modulus and Poisson's ratio for the proposed lattice materials.
- Numerical simulations reveal that elastic isotropy is nearly conserved in the inelastic large deformation response.
- For relative densities smaller than 1%, the metamaterial almost attains the upper bound of Poisson's ratio for an isotropic material, i.e $\nu = 0.5$.

3D lightweight mechanical metamaterial with nearly isotropic inelastic large deformation response

Xueyan Chen[a,b], Johnny Moughames[b], Qingxiang Ji[a,b], Julio Andrés Iglesias Martínez[b], Huifeng Tan[a*], Gwenn Ulliac[b],Vincent Laude[b], Muamer Kadic[b*]

[a] *National Key Laboratory of Science and Technology on Advanced Composites in Special Environments, Harbin Institute of Technology; 92 Xidazhi Street, Harbin, 150001, PR China*

[b] *Institut FEMTO-ST, CNRS, Université Bourgogne Franche-Comté, 25030 Besançon, France*

Abstract

Well-designed stretching-dominated lattices can form elastic metamaterials with high specific stiffness and strength. Their strongly anisotropic and unstable nonlinear mechanical properties, however, limit their application to energy absorption. In contrast, bending-dominated lattices are well known for high energy absorption capacity and stable nonlinear response, but poor elastic response. Here, we propose a new class of light-weight elastic isotropic bending-dominated truss lattice that combines both advantages. Numerical simulations reveal that the proposed lattices not only exhibit elastic isotropy, but also nearly isotropic inelastic large deformation response. In particular, for a relative density smaller than 1% the metamaterial almost attains the upper bound of Poisson's ratio for an isotropic material, i.e $\nu = 0.5$. Compared to BCC truss lattices, uniaxial compression tests show that the relative modulus is twice as large, and that the relative collapse strength and specific energy absorption are about 1.6 times as large. The designed metamaterial is thus a noteworthy alternative for load bearing, energy absorption, and transformation acoustics.

Keywords:
Bending-dominated, Mechanical metamaterial, Loading support, Energy absorption, Isotropy

1. Introduction

Metamaterials and lattice materials are attracting widespread interest due to their low weight and tailored mechanical properties, such as programmable deformations [1, 2], unusual acoustic properties [3, 4, 5, 6], controlled Poisson's ratio [7, 8, 9], reusable shock absorbing capacity [10, 11], high specific stiffness, specific strength and high energy absorption capacity [12, 13, 14]. These mechanical properties are largely determined by structural geometry and constituent materials [15, 16, 17, 18, 19, 20]. Recent advances in additive manufacturing have enabled the realization of mechanical materials at multi-length scales with a variety of base materials. Most well-designed lattice materials possess highly anisotropic mechanical properties, however,

*Corresponding author
Email addresses: tanhf@hit.edu.cn (Huifeng Tan[a]), muamer.kadic@univ-fcomte.fr (Muamer Kadic[b])

which limits their application to complicated cases, especially when the loading direction is non-deterministic.

The most popular method for designing isotropic structural materials is to combine different anisotropic structures with proper proportion, that is, to enhance the weaker directions and limit the stronger directions. Gurtner et al. presented a new class of optimal and isotropic three-dimensional truss lattice material [21]. Tancogne et al. enriched the isotropic truss-lattice family using combinations of elastically-anisotropic elementary cubic truss lattice and changing the ratio of bending-to-axial stiffness of the constituent beams [22, 23]. Lately, Bonatti et al. showed that a family of elastically-isotropic shell-lattice materials are always stiffer than optimal isotropic truss-lattices and approach the Hashin–Shtrikman bound at high relative densities [24].

According to theoretical predictions, only closed-cell materials can attain the Hashin–Shtrikman upper bounds on isotropic mechanical properties, even at ultra low relative density [25]. Numerically, Berger et al. identified a class of cubic-octet hybrid closed foams achieving the maximum isotropic stiffness [15]. By placing plates along the closest packed planes of crystal structures with cubic symmetry, Tancogne et al. presented a class of light-weight plate-lattices providing near isotropic yield strength together with elastic isotropy [26]. Crook et al. further introduced a class of plate nano-lattices that are the only materials to experimentally achieve the Hashin-Shtrikman and Suquet upper bounds for isotropic elastic stiffness and strength, respectively [27]. Similarly, by synthesizing $n + 1$ sets of continuous plates in a transversely quasi-periodic manner, a dual family of quasi-periodic mechanical metamaterials with extreme maximum isotropic stiffness were achieved in theory [28].

As stretching-dominated materials with low relative density, the structural lattices mentioned above exhibit a higher specific stiffness and strength, but a less stable nonlinear response than those deforming in a bending-dominated mode [29]. This is mainly because, in the initial elastic region, stretching-dominated materials store more strain energy during deformation than bending-dominated materials do. Under compression or tension, unlike bending-dominated materials, there exist micro-components in stretching dominated materials to support tensile forces and thus prevent displacements and rotations of nodes. When considering the nonlinear regime, things change drastically. In general, stretching-dominated materials lack stability toward large strain deformations and exhibit decreasing post-yield or post-buckling response. In contrast, bending-dominated materials make full use of plastic bending joints allowed for large deformations and provide relatively large and nearly constant stress in the nonlinear regime. Moreover, high specific stiffness and strength always come with large nonlinear anisotropy [21, 22, 23, 26]. Thus far and to best of our knowledge, however, few works have focused on designing isotropic nonlinear bending-dominated materials for energy absorption.

In this paper, a class of isotropic bending dominated truss lattice materials, formed by replacing the central connecting node of the body-centered cubic (BCC) truss lattice [30, 31, 32] with a simple cubic (SC) truss lattice element, is proposed for absorbing energy. The effects of geometrical parameters on the effective mechanical properties are analyzed using numerical simulations and an analytical theory. Results show that the designed metamaterials exhibit not only isotropic stiffness, but also nearly isotropic inelastic large deformation response. A series of samples with different relative densities are printed using two-photon polymerization in two different crystallographic directions, [100] and [110]. Uniaxial compression tests confirm the designed mechanical properties. Compared to BCC truss lattice materials, the designed metamaterials have a relative elastic modulus about twice as large and a specific energy absorption about 1.6 times as large.

2. Design of isotropic bending dominated lattice material

We first outline the general design procedure for combining the properties of BCC and SC truss lattices and achieving linear isotropy. As shown in Figures 1a and 1b, both lattices at low density are highly anisotropic and Young's modulus varies by more than 2 or 3 orders of magnitude as a function of the loading direction. The directions along which maxima occur, however, are different: they are the principal axes of the cubic unit cell for the SC lattice and its diagonals for the BCC lattice. The BCC-SC truss lattice is then defined by replacing the central connection of the BCC lattice with an element of the SC lattice, as Figure 1c depicts. The impact of struts on the mechanical behavior is indeed highly direction dependent. In the [100] direction, the struts of the inner SC lattice element enhance the overall mechanical properties, whereas the struts of the BCC lattice provide rotational degrees of freedom and thus guarantee the steadiness of the post-collapse response. In the [111] direction, the converse is true: mechanical properties are enhanced by the BCC struts whereas the post-collapse response is stabilized by the SC struts. As a result, isotropy can be achieved by adjusting the geometrical dimensions of the struts, as we show next. The relevant dimensions are the ratio of inner cubic strut length to unit cell length L_2/L and the ratio of strut diameter to unit cell length D/L (see Figures 1a). Both ratios influence the overall density of the structure $\bar{\rho}$. For compactness, we discuss their numerical values in the following, as obtained from numerical computations based on finite element analysis. A full analysis including analytical derivations is provided in the following section.

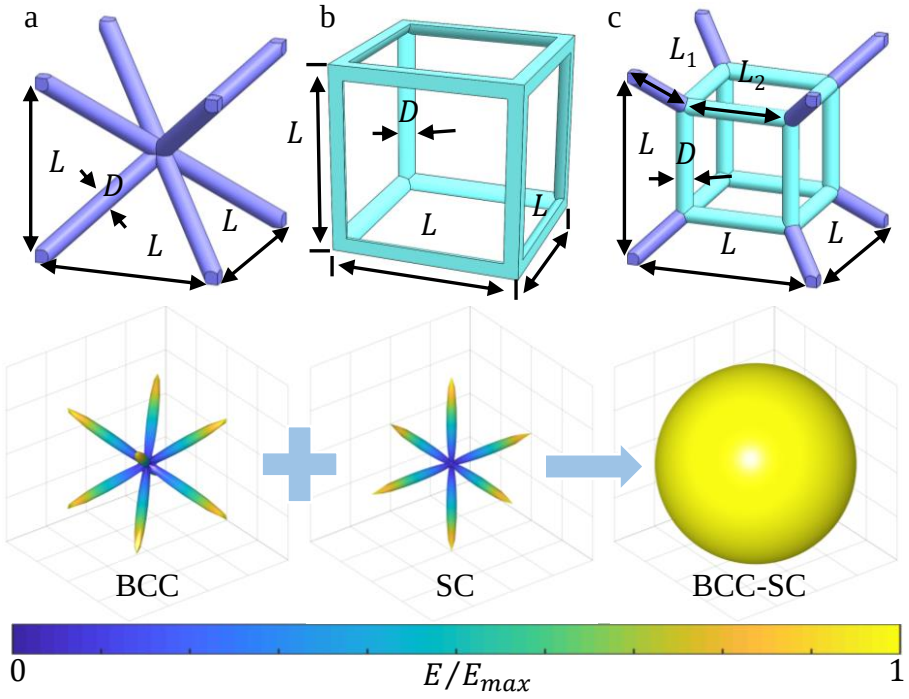

Figure 1: Linear elastic properties of cubic symmetric truss lattice materials. The representative unit cells and the corresponding normalized Young's modulus as a function of loading direction for (a) the BCC lattice, (b) the SC lattice, and (c) the BCC-SC lattice. The relative extreme values, $E_{\min}/E_{\max}$ are (a) 0.0249, (b) 0.0315 and (c) **1**.

2.1. Relative density

Figure 1a displays a non primitive cubic symmetric unit cell model of the body-centered cubic (BCC) lattice, composed of eight identical intersecting struts. Here, the struts are assumed to have uniform circular cross-section with constant radius R and length $l = \sqrt{3}L/2$, with L the side length of the cubic cell. For BCC truss lattice material, the relative density is defined as the ratio of the actual volume V occupied by the lattice structure to the total volume of the unit cell,

$$\bar{\rho} = \frac{V}{L^3}. \tag{1}$$

V is obtained by integration as

$$V = 8\left(\pi R^2 l - 2\sqrt{6}R^3\right). \tag{2}$$

Equation (1) can therefore be written

$$\bar{\rho} = 3\sqrt{3}\pi\left(\frac{R}{l}\right)^2 - 18\sqrt{2}\left(\frac{R}{l}\right)^3. \tag{3}$$

The above formula comprises two terms: the relative density of the ideal perfect struts minus the material overlap at nodes. The material overlap contribution increases with the aspect ratio R/l. For example, material overlap accounts for a correction by less than 5% when $R/l = 0.01$, but the correction reaches 50% for $R/l = 0.1$.

As shown in Fig.1c, the BCC-SC lattice is composed of 8 outer struts along diagonal directions with length L_1 and 12 inner struts along horizontal and vertical directions with length L_2. All struts have the same radius R. The volumes of outer and inner struts are

$$V_1 = \pi R^2 L_1 - C_1 R^3 \tag{4}$$

and

$$V_2 = \pi R^2 L_2 - C_2 R^3. \tag{5}$$

Constants C_1 and C_2 account for the overlap volume at nodes. Their numerical values were estimated using a 3D computer-aided design (CAD) software and are $C_1 = 3.35$ and $C_2 = 2.83$. The volume $V = 8V_1 + 12V_2$. The relative density of the BCC-SC lattice is given by

$$\bar{\rho} = 4\sqrt{3}\pi\left(\frac{R}{L}\right)^2 + (12 - 4\sqrt{3})\pi\left(\frac{R^2 L_2}{L^3}\right) - C\left(\frac{R}{L}\right)^3 \tag{6}$$

with $L = L_2 + \frac{2}{\sqrt{3}}L_1$ the unit cell length. The numerical value of the last constant is $C = 8C_1 + 12C_2 = 60.73$. The relative density is determined by two independent variables, for instance the ratio of radius to unit cell length R/L and the ratio of inner strut length to unit cell length L_2/L. One can use equally well D/L and L_2/L as the independent variables, with $D = 2R$ the diameter of the struts. For a given relative density, only one of the two variables needs to be adjusted to regulate the mechanical properties of the BCC-SC lattice. Figure 2 illustrates the relationship between relative density and the geometrical ratios. It is obvious that the relative density will increase as either R/L or L_2/L increases.

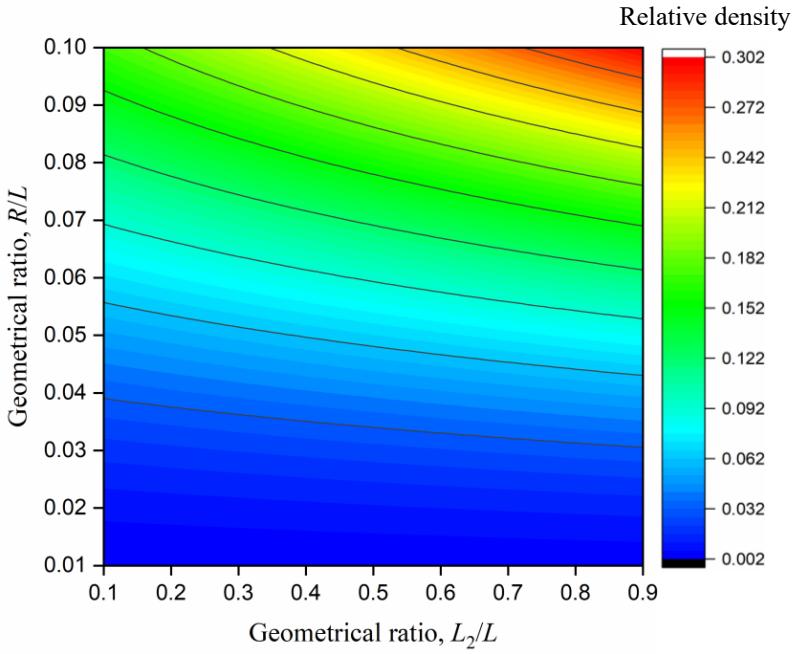

Figure 2: Contour plot of the relative density of BCC-SC truss lattices versus geometrical parameters D/L and L_2/L.

2.2. *Elastic behavior of BCC and BCC-SC lattices*

In a Cartesian coordinate system, the constitutive law of linear elasticity relates the strain tensor $\boldsymbol{\varepsilon}$ to the stress tensor $\boldsymbol{\sigma}$ via a fourth-order symmetric elastic compliance tensor $\mathbf{S}$, as

$$\boldsymbol{\varepsilon} = \mathbf{S} : \boldsymbol{\sigma}. \tag{7}$$

For cubic-symmetric lattice materials, there are only three independent elements in the compliance matrix, i.e.

$$\boldsymbol{S} = \begin{bmatrix} 1/E & -\upsilon/E & -\upsilon/E & 0 & 0 & 0 \\ & 1/E & -\upsilon/E & 0 & 0 & 0 \\ & & 1/E & 0 & 0 & 0 \\ & & & 1/G & 0 & 0 \\ & \text{sym} & & & 1/G & 0 \\ & & & & & 1/G \end{bmatrix}. \tag{8}$$

E, G and υ are Young's modulus, the shear modulus and Poisson's ratio of the lattice material in principal directions. Detailed analytical derivations for BCC and BCC-SC lattices are given in the following section.

As depicted in Figure 3b, micro-struts have an irregular geometry at both ends and hence their mechanical behavior around nodes has to be quite complex. Strictly speaking, traditional theoretical analysis based on perfect beam theory is not applicable in such a case. To overcome

this issue and for the sake of generality, irregular struts are effectively replaced by perfect cylinders with the same volume. Thus, an effective strut length is introduced instead of the original strut length. Table 1 gives the values of effective strut lengths for both BCC and BCC-SC lattices.

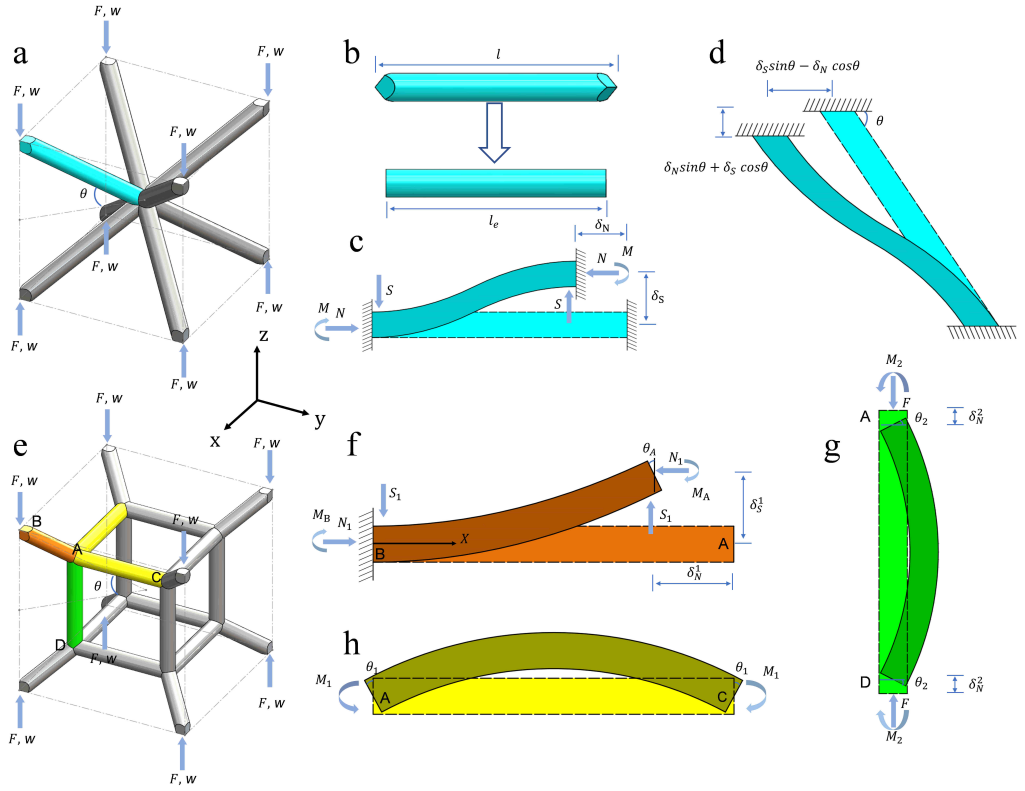

Figure 3: Representative unit cells of (a) the BCC lattice and (e) the BCC-SC lattice under uniaxial compression. (b) Effective cylindrical model for an irregular strut. Panels (c)-(g) illustrate the corresponding simplified mechanical beam model.

Table 1: Effective strut length for BCC and BCC-SC lattices.

Topology	l_e	l_1	l_2
BCC	$l - 2\sqrt{6}R/\pi$		
BCC-SC		$L_1 - C_1R/\pi$	$L_2 - C_2R/\pi$

2.2.1. Compressive modulus and Poisson ratio of BCC lattice

Due to cubic symmetry, one strut of the unit cell is selected for further analysis, as shown in Figure 3c. When the unit cell is under uniaxial compression, both ends of the micro-strut are able to move in the principal directions. Figure 3c illustrates the deformation of the strut under compression. The strut can be considered as a clamped-clamped beam subjected to an axial force, a shear force and a bending moment. Based on Timoshenko's beam theory, and in a

reference frame attached to the beam, the axial displacement δ_N and the shear deflection δ_S are given by

$$\delta_N = \frac{N l_e}{E_s A}, \tag{9}$$

$$\delta_S = \frac{S l_e^3}{12 E_s I}\left(1 + \frac{12 E_s I}{\kappa A G_s l_e^2}\right) = \frac{S k l_e^3}{12 E_s I}, \tag{10}$$

where N and S are the axial force and the shear force applied to the strut, l_e is the effective length of the strut, E_s is the elastic modulus of the strut material, $A = \pi R^2$ is the cross section area of the strut, $I = \pi R^4/4$ is the second moment of area of the beam, G_s is the shear modulus of the strut material, and κ is Timoshenko's shearing coefficient. The coefficient k is introduced to incorporate both bending and shearing coupling effects.

For a circular strut, κ is obtained by the following expression [33]

$$\kappa = \frac{6(1+\nu_s)^2}{7 + 12\nu_s + 4\nu_s^2}, \tag{11}$$

where ν_s is Poisson's ratio of the strut material. For an isotropic material, we further have

$$\frac{E_s}{2G_s(1+\nu_s)} = 1. \tag{12}$$

As a result, the above equations lead to

$$\delta_N = \frac{N l_e}{\pi E_s R^2}, \tag{13}$$

$$\delta_S = \frac{k S l_e^3}{3\pi E_s R^4}, \tag{14}$$

$$k = 1 + \frac{7 + 12\nu_s + 4\nu_s^2}{1+\nu_s}\left(\frac{R}{l_e}\right)^2. \tag{15}$$

The forces N and S originate from a global force F oriented along direction [001]:

$$N = F\sin\theta, \tag{16}$$

$$S = F\cos\theta, \tag{17}$$

with $\sin\theta = 1/\sqrt{3}$ and $\cos\theta = \sqrt{2/3}$. θ is the angle between directions [110] and [001]. The global displacements u, v and w of the unit cell in the x, y and z directions, respectively, can then be expressed as

$$u = v = \frac{1}{\sqrt{2}}(\delta_S \sin\theta - \delta_N \cos\theta) = \frac{1}{3}\left(\frac{k F l_e^3}{3\pi E_s R^4} - \frac{F l_e}{\pi E_s R^2}\right), \tag{18}$$

$$w = -(\delta_S \cos\theta + \delta_N \sin\theta) = -\frac{1}{3}\left(\frac{2k F l_e^3}{3\pi E_s R^4} + \frac{F l_e}{\pi E_s R^2}\right). \tag{19}$$

The effective Young's modulus E and Poisson's ratio ν of the BCC lattice material, therefore, are given by

$$E = \frac{\sigma_z}{\varepsilon_z} = \frac{\frac{-4F}{L^2}}{\frac{2w}{L}} = \frac{9\sqrt{3}\pi E_s}{3 + 2k\left(\frac{l_e}{R}\right)^2}\frac{R^2}{l_e l}, \tag{20}$$

$$\nu = -\frac{u}{w} = \frac{k - 3\left(\frac{R}{l_e}\right)^2}{2k + 3\left(\frac{R}{l_e}\right)^2}. \tag{21}$$

The expression for Young's modulus considers the mid-plane symmetry of the BCC unit cell, so that the force F is distributed over 4 struts (hence the vertical stress is expressed as $\sigma_z = -4F/L^2$) and the strain is symmetrical with respect to the cell center (hence $\varepsilon_z = 2w/L$).

2.2.2. [100] Shear modulus of BCC lattice

Consider the BCC unit cell sketched in Figure 4a with an applied shear displacement. The strut can also be treated as a clamped-clamped beam. The local displacement δ_N and δ_S, and the corresponding force N and S, are related to the global shear displacement u and global force F via

$$\delta_N = \sqrt{2}u\cos\theta = \frac{2}{\sqrt{3}}u, \tag{22}$$

$$\delta_S = \sqrt{2}u\sin\theta = \frac{\sqrt{2}}{\sqrt{3}}u, \tag{23}$$

$$N\cos\theta + S\sin\theta = \sqrt{2}F. \tag{24}$$

By substituting Eq. (13), (14), (22) and (23) into (24), we obtain

$$F = \left(\frac{2\pi E_s R^2}{l_e} + \frac{3\pi E_s R^4}{k l_e^3}\right)\frac{u}{3}. \tag{25}$$

Therefore, the effective shear modulus of the BCC lattice is

$$G = \frac{\tau}{\gamma} = \frac{\frac{F}{L^2}}{\frac{u}{L}} = \frac{\pi E_s}{3}\left(2 + \frac{3}{k}\left(\frac{R}{l_e}\right)^2\right)\frac{R^2}{l_e L}. \tag{26}$$

2.2.3. Bulk modulus of BCC lattice

Under hydrostatic pressure, the standard strut can again be considered a clamped-clamped beam subjected to an axial force. Based on Timoshenko's beam theory, we have

$$\delta = \frac{N l_e}{E_s A}. \tag{27}$$

The global force F and the displacement u are given by

$$N = \sqrt{3}F, \tag{28}$$

$$\delta = \sqrt{3}u. \tag{29}$$

We get an analytical expression for the bulk modulus from the definition

$$K = -\frac{dP}{dV/V} = \frac{2\pi E_s R^2}{l_e L\left(3 - 6\frac{u}{L} + 4\frac{u^2}{L^2}\right)}, \tag{30}$$

with $dP = 4F/L^2$, $V = L^3$, and $dV = L^3 - (L - 2u)^3$. Noting that $u \ll L$, we simply have

$$K \approx \frac{2\pi E_s R^2}{3l_e L}. \tag{31}$$

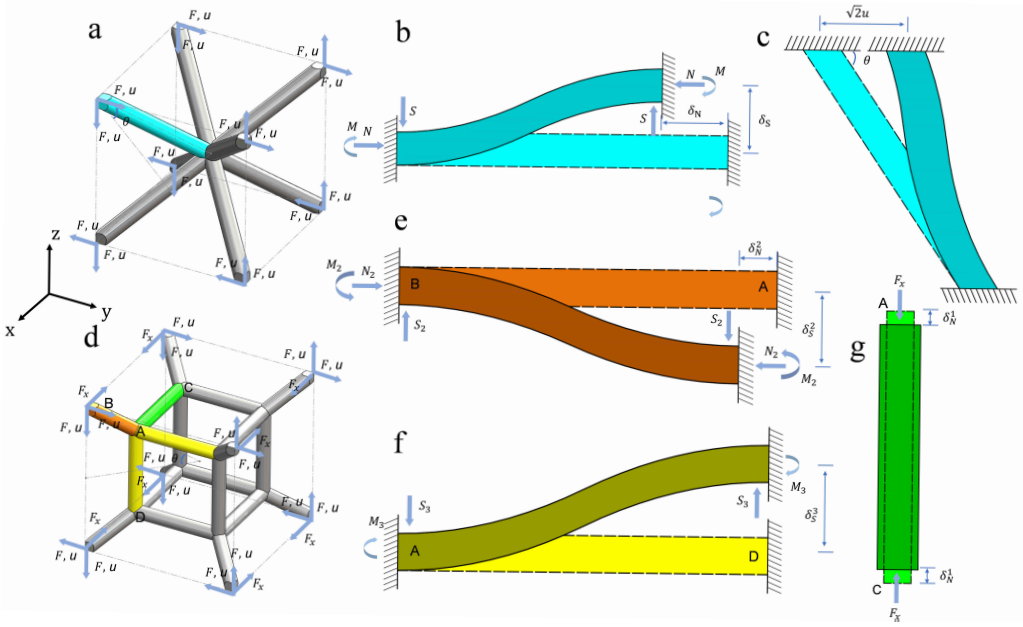

Figure 4: (a)-(c) Deformation of struts in BCC unit models under pure shear loading.(d)-(g) Three different representive simplied beam models for BCC-SC lattice subjecting to pure shearing force.

2.2.4. *Elastic modulus and Poisson ratio of BCC-SC lattice*

Different from the BCC lattice, when under compression the struts of the BCC-SC lattice can not be simply considered as clamped-clamped beams. As sketched in Figure 3e, struts can be divided into three types, labeled AB, AC or AD according to their deformation behavior. Strut AB can be considered as a clamped-free beam (A is free and B is clamped) subjected to an axial force, a shear force and a bending moment. Based on the moment balance principle of statics,

$$M_A + M_B = S_1 l_1, \tag{32}$$

$$M(x) = S_1 l_1 - M_A - S_1 x. \tag{33}$$

It follows that $M_A = -M(l_1)$ and $M_B = M(0)$. The relative rotation between the ends of the beam sketched in Figure 3f is calculated from the beam equation

$$\theta_A = \int_0^{l_1} \frac{M(x)}{E_s I} dx = \frac{l_1}{E_s I}\left(\frac{S_1 l_1}{2} - M_A\right). \tag{34}$$

Strut AC is only subject to a constant bending moment M_1 and thus the relative rotation at point A is given by

$$\theta_1 = \frac{M_1 l_2}{2E_s I}. \tag{35}$$

Strut AD is subject to a constant bending moment M_2 and an axial force F and thus the relative rotation at point A is given by

$$\theta_2 = \frac{M_2 l_2}{2E_s I}. \tag{36}$$

Due to the fact that all struts are connected at a same rigid joint A, they must experience the same rotation and moment balance

$$\theta_A = \theta_2 = \sqrt{2}\theta_1, \tag{37}$$

$$M_A = M_2 + \sqrt{2}M_1. \tag{38}$$

Substituting these beam equations into the balance equations,

$$M_A = k_1 S_1 l_1, \tag{39}$$

$$k_1 = \frac{2l_1}{l_2 + 4l_1}. \tag{40}$$

We have, by Timoshenko's beam theory

$$\delta_N^1 = \frac{N_1 l_1}{E_s A}, \tag{41}$$

$$\delta_S^1 = \frac{k_2 S_1 l_1^3}{E_s I}, \tag{42}$$

$$k_2 = \frac{2 - 3k_1}{6} + \frac{E_s I}{\kappa A G_s l_1^2}, \tag{43}$$

$$\delta_N^2 = \frac{F l_1}{2E_s A}. \tag{44}$$

Thus, the relationship between global displacement and global force is

$$u_1 = v_1 = \frac{1}{\sqrt{2}}\left(\delta_S^1 \sin\theta - \delta_N^1 \cos\theta\right) = \frac{1}{3}\left(\frac{k_2 F l_1^3}{E_s I} - \frac{F l_1}{E_s A}\right), \tag{45}$$

$$w_1 = -\left(\delta_S^1 \cos\theta + \delta_N^1 \sin\theta + 2\delta_N^2\right) = -\frac{1}{3}\left(\frac{4k_2 F l_1^3}{E_s I} + \frac{2Fl_1}{E_s A} + \frac{3Fl_2}{E_s A}\right). \tag{46}$$

The effective Young's modulus and Poisson's ratio of the BCC-SC lattice are finally obtained as

$$E = \frac{\sigma_z}{\varepsilon_z} = \frac{\frac{-4F}{L^2}}{\frac{w_1}{L}} = \frac{12\pi E_s}{3 + \frac{2l_1}{l_2} + 16k_2\left(\frac{l_1}{R}\right)^2 \frac{l_1}{l_2}} \left(\frac{R}{l_2}\right)^2 \frac{l_2}{L}, \tag{47}$$

$$\nu = -\frac{2u_1}{w_1} = \frac{\frac{8k_2 l_1^2}{R^2} - 2}{2 + \frac{16k_2 l_1^2}{R^2} + \frac{3l_2}{l_1}}. \tag{48}$$

In addition, in case the BCC-SC lattice material has cubic symmetry, the bulk modulus can be obtained as a function of Young's modulus and the shear modulus as

$$K = \frac{E}{3(1-2\nu)}. \tag{49}$$

2.2.5. [100] Shear modulus of BCC-SC lattice

Figure 4 illustrates the way micro-struts deform under a pure shear displacement. For strut AB, only axial displacement occurs during deformation, thus

$$F_x = \frac{2E_s A \delta_N^1}{l_2}. \tag{50}$$

Strut AC can be considered as a beam with clamped-clamped boundary conditions and by virtue of Timoshenko's beam theory we have

$$\delta_N^2 = \frac{N_2 l_1}{E_s A}, \tag{51}$$

$$\delta_S^2 = \frac{k_3 S_2 l_1^3}{12 E_s I}, \tag{52}$$

$$k_3 = 1 + \frac{7 + 12\nu_s + 4\nu_s^2}{1 + \nu_s}\left(\frac{R}{l_1}\right)^2. \tag{53}$$

The strut force and displacement can be expressed in terms of the macroscopic force and displacement as

$$N_2 = \sqrt{2}F\cos\theta + F_x \sin\theta = \frac{2F}{\sqrt{3}} + \frac{F_x}{\sqrt{3}}, \tag{54}$$

$$S_2 = \sqrt{2}F\sin\theta - F_x\cos\theta = \frac{\sqrt{2}F}{\sqrt{3}} - \frac{\sqrt{2}F_x}{\sqrt{3}}, \tag{55}$$

$$\delta_N^2 = \sqrt{2}u\cos\theta - \delta_N^1\sin\theta = \frac{2u}{\sqrt{3}} - \frac{\delta_N^1}{\sqrt{3}}, \tag{56}$$

$$\delta_S^2 = \sqrt{2}u\sin\theta + \delta_N^1\cos\theta = \frac{\sqrt{2}u}{\sqrt{3}} + \frac{\sqrt{2}\delta_N^1}{\sqrt{3}}. \tag{57}$$

Those equations lead to

$$u - \left(\frac{1}{2} + \frac{l_1}{l_2}\right)\delta_N^1 = \frac{l_1}{A}\frac{F}{E}, \tag{58}$$

$$u + \left(1 + \frac{k_3 l_1^3 A}{6 I l_2}\right)\delta_N^1 = \frac{k_3 l_1^3}{12 I}\frac{F}{E}. \tag{59}$$

Solving those equations, we get

$$u = \frac{k_4 F l_1}{E\pi R^2}, \tag{60}$$

$$k_4 = \frac{1 + k_3\left(\frac{1}{6} + \frac{l_1}{l_2}\right)\left(\frac{l_1}{R}\right)^2}{\frac{3}{2} + \left(1 + \frac{2}{3}k_3\left(\frac{l_1}{R}\right)^2\right)\frac{l_1}{l_2}}. \tag{61}$$

Strut AD is subject to a shear force and a bending moment. Its deflection is given by

$$\delta_S^3 = \frac{k_5 S l_2^3}{3\pi E_s R^4}, \tag{62}$$

$$k_5 = 1 + \frac{7 + 12\nu_s + 4\nu_s^2}{1 + \nu_s}\left(\frac{R}{l_2}\right)^2. \tag{63}$$

Finally, the effective shear modulus is given by

$$G = \frac{\tau}{\gamma} = \frac{\frac{4S}{L^2}}{\frac{2\left(2u + \delta_S^3\right)}{L}} = \frac{2\pi E_s}{2k_4 + \frac{k_5}{3}\left(\frac{l_2}{R}\right)^2\frac{l_2}{l_1}}\left(\frac{R}{l_1}\right)^2\frac{l_1}{L}. \tag{64}$$

2.3. Identification of isotropy

An analytical expression for Young's modulus along an arbitrary direction can be obtained as [34]:

$$\frac{1}{E_{ijk}} = \frac{1}{E} - \frac{1}{G}(Z-1)\left(l_{i1}^2 l_{j2}^2 + l_{j2}^2 l_{k3}^2 + l_{i1}^2 l_{k3}^2\right), \tag{65}$$

where $[ijk]$ is the loading direction, and l_{i1}, l_{j2} and l_{k3} are direction cosines between the $[ijk]$ direction and the three principal directions. Zener's ratio Z, which is used to quantify the anisotropy of cubic crystals, is

$$Z = \frac{2(1+\upsilon)G}{E}, \tag{66}$$

By substituting Eq. (47), Eq. (48) and Eq. (64) into Eq. (66), Zener's ratio for the BCC-SC lattice can expressed as

$$Z = \frac{8k_2(\frac{l_1}{R})^2 + \frac{l_2}{l_1}}{2k_4 + \frac{k_5}{3}(\frac{l_2}{R})^2(\frac{l_2}{l_1})}. \tag{67}$$

When $Z = 1$, a cubic material is exactly elastically isotropic. Finally, a combination of Eq. (6) and Eq. (67) will help us identifying the suitable geometrical parameters for isotropy.

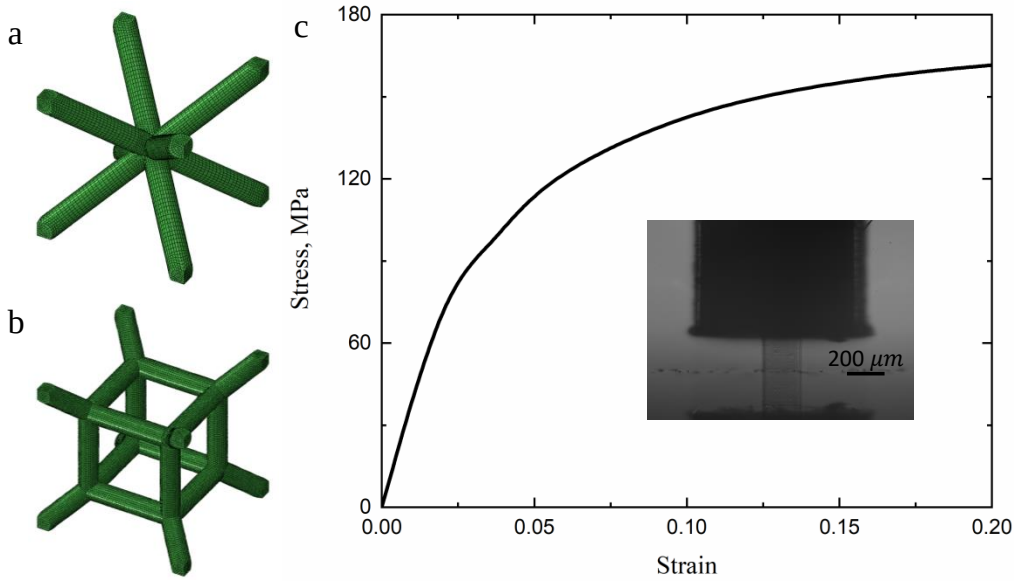

Figure 5: Representative numerical unit cell models for (a) BCC and (b) BCC-SC truss lattices. (c) The engineering stress-strain curve of material IP-S is obtained from compression experiments.

3. Numerical study

3.1. Simulation

To obtain the mechanical response of BCC and BCC-SC truss lattices, a series of unit cell models with different relative densities ranging from 1 to 20% were built using the commercial finite element software ABAQUS. To ensure the calculation accuracy, as shown in Figure 5, there exist at least fourteen three dimensional linear solid elements (type C3D8R) along the strut diameter direction. IP-S polymer is chosen as constituent material for simulations. The constituent material was modeled as an isotropic elasto-platic material with Young's modulus 3.6 GPa and Poisson's ratio 0.35 following an isotropic strain hardening behavior. A 0.2% offset strength of 81 Mpa is taken as yield strength. The detailed engineering stress-strain curve shown in Figure.5 is from a compression experiment on a micro-cube. For all models, the edge length of unit cells was fixed to 200 μm. The strut diameter was changed with the relative density, as well as the

other geometrical parameters of the BCC-SC lattice. Periodic boundary conditions were applied by matching mesh nodes on opposite planes with linear constraint equations [35]. Independent elastic moduli together with Poisson's ratio were extracted from uniaxial compression numerical experiments along the principal compression direction and along the two pure shear directions, respectively.

3.2. Effect of geometrical parameter on elastic properties

Figure 6a considers a fixed value of the effective density $\bar{\rho} = 0.2$, leaving the ratio L_2/L as the only variable for optimization. The BCC-SC lattice is obtained as a continuous morphing operation as L_2/L varies from 0 (BCC) to 1 (SC). Significantly, Zener's ratio Z decreases from a value larger than 1 to a value close to 0; by continuity, there is a single value $L_2/L = 0.545$ for which $Z = 1$ and linear isotropy is achieved. Young's modulus E increases steadily as a function of L_2/L, whereas the shear modulus G first decreases until $L_2/L = 0.8$ after which point it increases slightly. Hence, the BCC-SC lattice achieves a trade-off between the elastic properties of the BCC lattice, that favors the shear modulus G, and those of the SC lattice, that optimizes Young's modulus E.

The same procedure can be repeated for different values of the effective density $\bar{\rho}$. Figure. 6b displays the value of ratio L_2/L that is needed to guarantee isotropy ($Z = 1$) as density varies. Theoretical predictions are slightly lower than simulation results. In the range $\bar{\rho} \in [0 : 0.2]$ its variation is almost linear and a linear regression can be performed. As a whole, Figure. 6b provides a map of the geometrical parameters that define the linear isotropic BCC-SC truss lattice family.

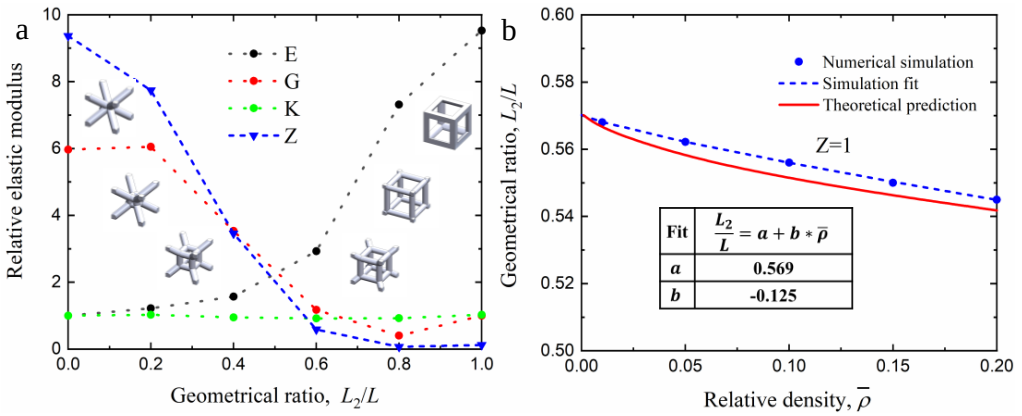

Figure 6: (a)Effect of geometrical parameter on elastic modulus and isotropy for a relative density of 0.2. (b) Evolution of ratio of inner strut length to unit cell length as a function of relative density obtained by theory, simulation and curve fitting.

3.3. Elastic properties

Figure 7 depicts comparison of relative stiffness, relative shear modulus, relative bulk modulus and Poisson's ratio obtained from numerical simulation and analytical theory (see Supporting Information) for BCC lattice and BCC-SC lattice. For all elastic properties, the analytical predictions which account for nodal effect and bending effect are in good agreement with simulations.

Observed that both BCC lattice and BCC-SC lattice are bending-dominated. The stiffness of the BCC-SC lattice is at least twice as large as that of the BCC lattice. Conversely, the shear modulus of the BCC lattice is always larger than that of the BCC-SC lattice for relative densities of up to 0.2. Having a similar deformation mode with the BCC lattice, the BCC-SC lattce always possess nearly the same bulk modulus as the BCC lattice. Poisson's ratio of both configurations

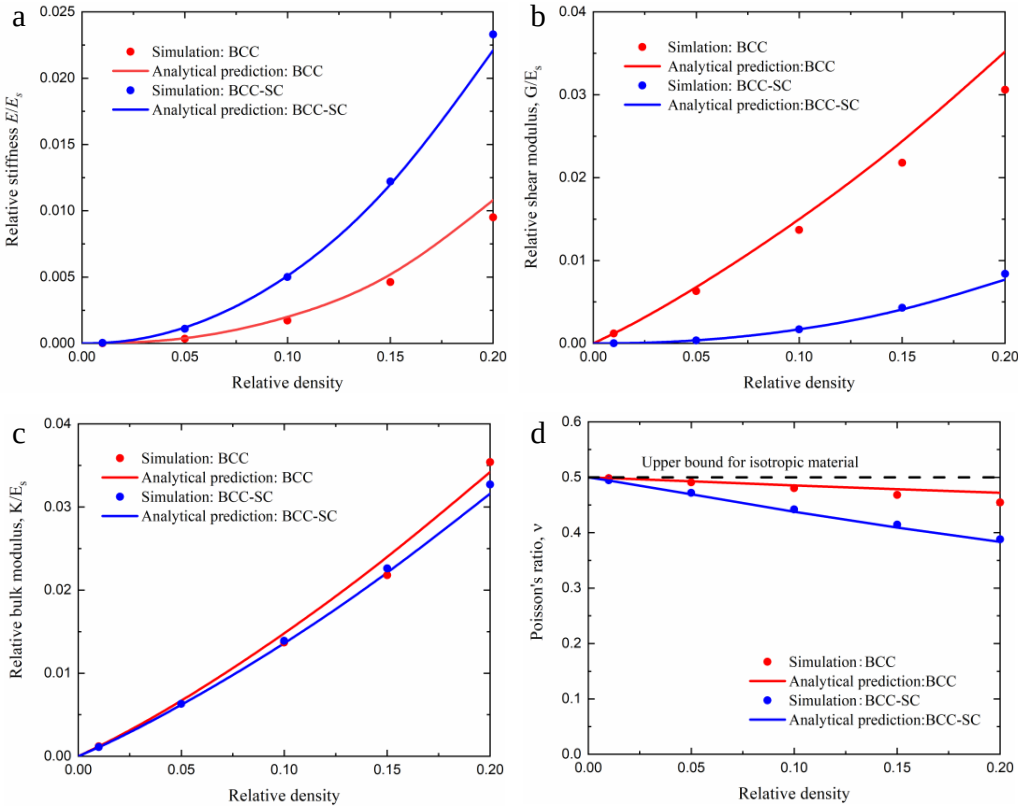

Figure 7: Comparison of relative elastic properties from simulations and analytical theory for BCC lattice and BCC-SC lattice.

are also presented in Figure 7d. It is clear that the Poisson's ratio of BCC lattice is always larger than that of BCC-SC lattice. For both configurations, the Poisson's ratio decreases as relative density increases. In particular, the isotropic BCC-SC lattice with a relative density of 0.01 have a Poisson's ratio which almost attains the upper bound, 0.5, for isotropic material. This value of the effective Poisson's ratio leads to a fairly large ratio of bulk modulus to shear modulus of about $K/G = 90.6$, making the elastically isotropic BCC-SC lattice an interesting structural basis in the field of transformation elastodynamics (see Supporting Information).

3.4. Inelastic large deformation response and nonlinear isotropy

To investigate the nonlinear response of both configurations, a large engineering strain of -0.2 is applied on corresponding numerical models along [100], [110] and [111] directions. Figure.8 show the stress-strain response of BCC-SC lattices with different relative densities, obtained

along the three principal directions [100], [110] and [111]. For comparison purposes, the full range covered by the stress-strain response of BCC lattices for all loading directions is added. It can be observed that BCC lattice display a very anisotropic nonlinear response, whereas the anisotropy of the BCC-SC lattice remains quite limited. For relative density ranging from 0.01 to 0.2, the strongest direction and weakest direction of BCC-SC lattice are [111] and [100], respectively. In all loading directions, the isotropic BCC-SC lattice exhibits an elastic response followed by a weakly increasing elastic-plastic behavior and a nearly constant stress plateau, which is similar to BCC lattice in [100] direction. With an applied uniaxial strain up to 0.1, their deformation and stress distribution are presented in Figure.8e. During deformation, plastic bending hinges along with stress concentration occur around the nodes. It should be noted that the distribution of plastic bending hinges of the isotropic BCC-SC lattice are highly loading-direction depended. Plastic bending hinges can be found at the ends of diagonal struts for [100] direction and inner SC struts for [110] direction and [111] direction. This implies that the combination of inner SC lattice and outer BCC lattice provide sufficient rotational degrees of freedom and guarantee the occurrence of plastic bending hinges regardless of loading direction. Bending-dominated lattices are always failed by bending collapse rather than yield or buckling. As pointed out by Gumruka et al. [31], the collapse strength of bending-dominated lattices can be calculated from the intersection point of the elastic–plastic collapse and the plastic collapse regions. The collapse strength σ_c is here defined empirically as the value of the engineering stress where strain equals 0.1. All of them have been highlighted in stress-strain curves as colored dots. For a fair comparison between different configurations, collapse strength in [100] direction are selected. The evolution of the relative collapse strength as a function of the relative density is shown in Fig.9.

It is observed that the collapse strength of both configurations scales non-linearly with relative density. The BCC-SC lattice always has a higher relative compressive strength. For relative density around 0.2, the BCC-SC lattice has a relative strength about 1.6 times and a relative elastic modulus about 2.1 times larger than those of the BCC lattice.

Using the previous design rules, only elastic isotropy is valid for small strain. However, for applications in energy absorption and load bearing, it is also important to quantify nonlinear anisotropy. In this respect, the collapse strength and the specific energy absorption (SEA) are the most important aspects for 3D energy absorbing metamaterials. They are respectively used to evaluate the load bearing capacity and the entire energy absorption of a structural lattice. The SEA is defined as the work performed by a uniaxial compression up to constant strain ε_0, taken as 0.2 for simulations, 0.2 and 0.5 for experiments, normalized by the total mass

$$\mathrm{SEA} = \frac{V \int_0^{\varepsilon_0} \sigma d\varepsilon}{M}. \tag{68}$$

In this work, we consider that nonlinear isotropy is achieved when both collapse strength and SEA are constant regardless of the loading direction. Nonlinear anisotropy is quantified by the ratios $\sigma_c^{\max}/\sigma_c^{\min}$ and $\mathrm{SEA}^{\max}/\mathrm{SEA}^{\min}$, where minima and maxima are taken over all loading directions in 3D space.

To check these mechanical properties, elasto-plastic solid elements simulations with compressive loading along 91 different directions spanning the irreducible Brillouin zone were conducted [36, 26]. Figure 10(a,b) summarize in the form of pole figures the dependence of collapse strength and specific energy absorption with loading direction for the BCC-SC lattice with $\bar{\rho} = 0.1$. The largest nonlinear anisotropy ratios are $\sigma_c^{\max}/\sigma_c^{\min} = 1.08$ and $\mathrm{SEA}^{\max}/\mathrm{SEA}^{\min} = 1.09$.

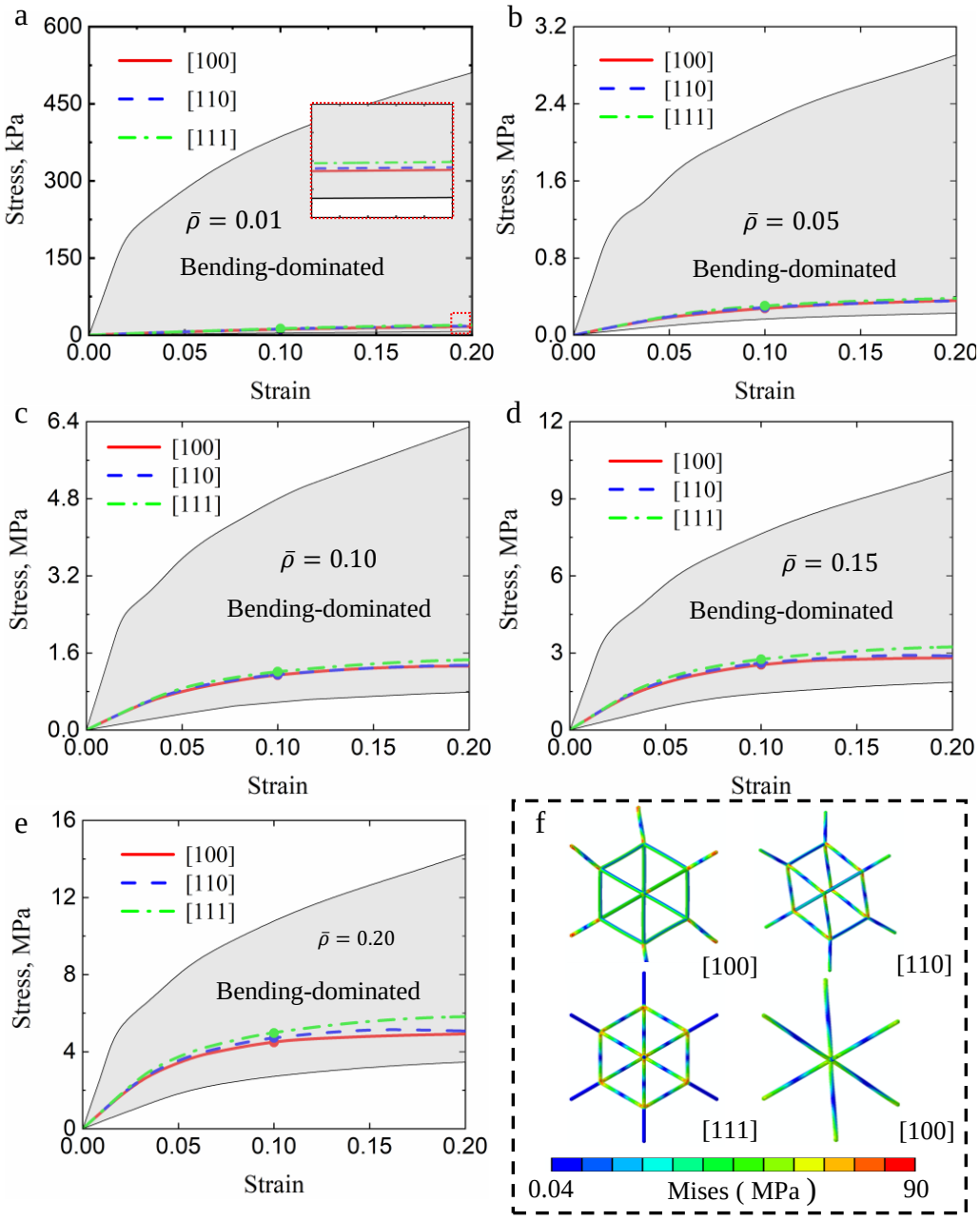

Figure 8: Nonlinear elastic properties of BCC-SC truss lattice materials. (a-e) The nonlinear compressive response is shown for different relative densities, ranging from 0.01 to 0.2 and computed along the [100], [110], and [111] directions. The light gray area outlines the range covered by the response of BCC lattices for all loading directions. (f)At a relative density of 0.01, contour plots illustrate the distribution of stress for the isotropic BCC-SC lattice along the [100], the [110] and the [111] directions and the BCC lattice along the [100] direction. The applied strain is 0.1 in all cases. Detailed deformation frames are shown in Figure S1.

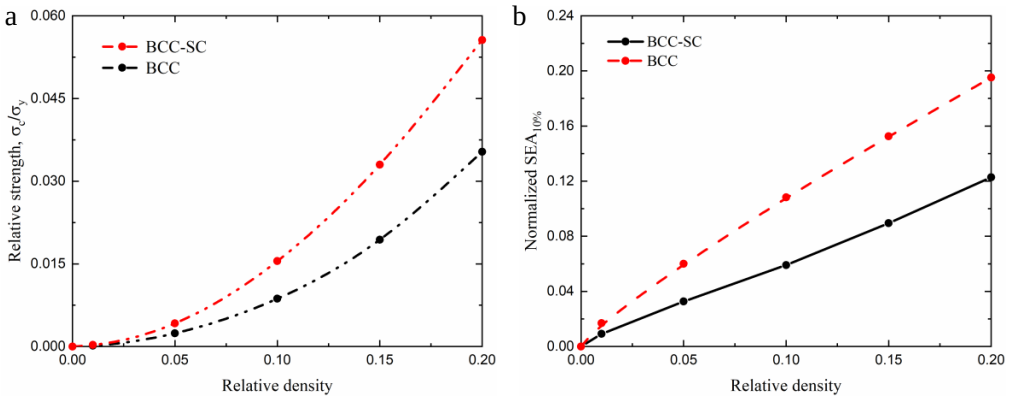

Figure 9: Evolution of (a) the relative collapse strength and (b) the normalized SEA as a function of relative density.

The softest direction is $[12, 4, 1]$, whereas the strongest direction is [111]. Similar trends are found for other relative densities. The largest nonlinear anisotropy ratios are summarized by Figure 10c as a function of relative density. They initially decrease with the relative density to reach their minima for $\bar{\rho} = 0.1$, after which value they increase only slightly.

For most values of the relative density, both nonlinear anisotropy ratios remain below 1.1, implying very limited nonlinear anisotropy. Even in the worst case, the nonlinear anisotropy ratios compare favourably with the case of other lattices displaying elastic isotropy [21, 23, 24]. That property makes the BCC-SC truss lattice a noteworthy alternative for load bearing and energy absorption.

4. Experiment

Samples were fabricated using a liquid photoresist (IP-S, Nanoscribe GmbH) and a commercial three-dimensional lithography system (Photonics Professional, Nanoscribe GmbH). The laser beam was focused by using a dip-in ×63 objective lens with 1.4 numerical aperture. A Galvanometric scan speed of 10 m/s was used for the whole fabrication process. After polymerization was achieved, the sample was developed in a PGMEA (1-methoxy-2-propanol acetate) solution for 20 minutes to remove the unexposed photoresist.

In order to validate the design of the BCC-SC truss lattice, samples with different relative densities $\bar{\rho} = 0.01$, 0.05, 0.1, 0.15, and 0.2 were fabricated by direct laser writing. To reliably obtain the actual geometrical parameters of samples, Scanning electron micrograph (SEM) images are shown in Figure 11. The measured relative densities via SEM images for samples are $\bar{\rho} = 1.4\%$, 5.9%, 10.8%, 15%, and 21.1%, respectively. Both crystallographic directions [100] and [110] were considered to investigate the dependence of the compressive response with loading direction. Table S2 summarizes the geometrical parameters of the printed samples.

Under compression, samples are placed between a fixed glass substrate and a flat loading stamp driven with a stepping motor. Position was read directly from the linear stage. In addition, the true strain was obtained via image cross correlation from a digital camera equipped with a 20× objective lens facing the sample to monitor the deformation of the lateral faces of the sample under compression test.

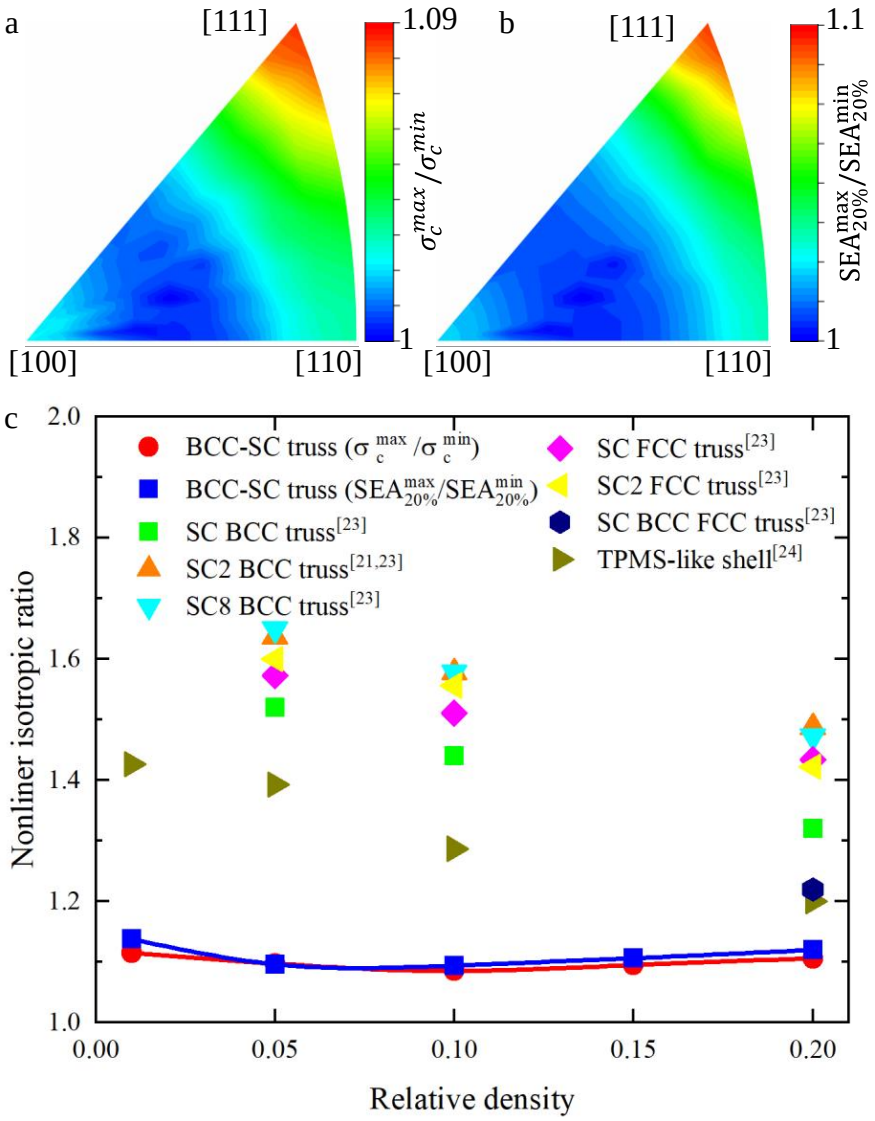

Figure 10: Pole figures for directional denpendency of (a) bending collapse strength distribution and (b) specific energy absorption distribution of the proposed mechanical metamaterial with a relative density of 0.1. (c) Comparison of nonlinear isotropic ratios between the proposed BCC-SC truss lattice and other elastic isotropic truss lattices and nearly isotropic TPMS-like shell lattice..

Figure 12 summarizes the compressive stress-strain curves and acquired deformation frames obtained experimentally with the different samples. For all relative densities, the experimental and numerical compressive responses show similar trends (see Figure S2). The [100] sample for $\bar{\rho}$ = 1.4% first deforms elastically but then follows a weakly nonlinear and increasing behavior (see Figure 12a). After reaching the first peak stress of about 20 kPa at a strain of 0.1, the response of the sample retains almost-periodic buckling oscillations. The sample collapses from

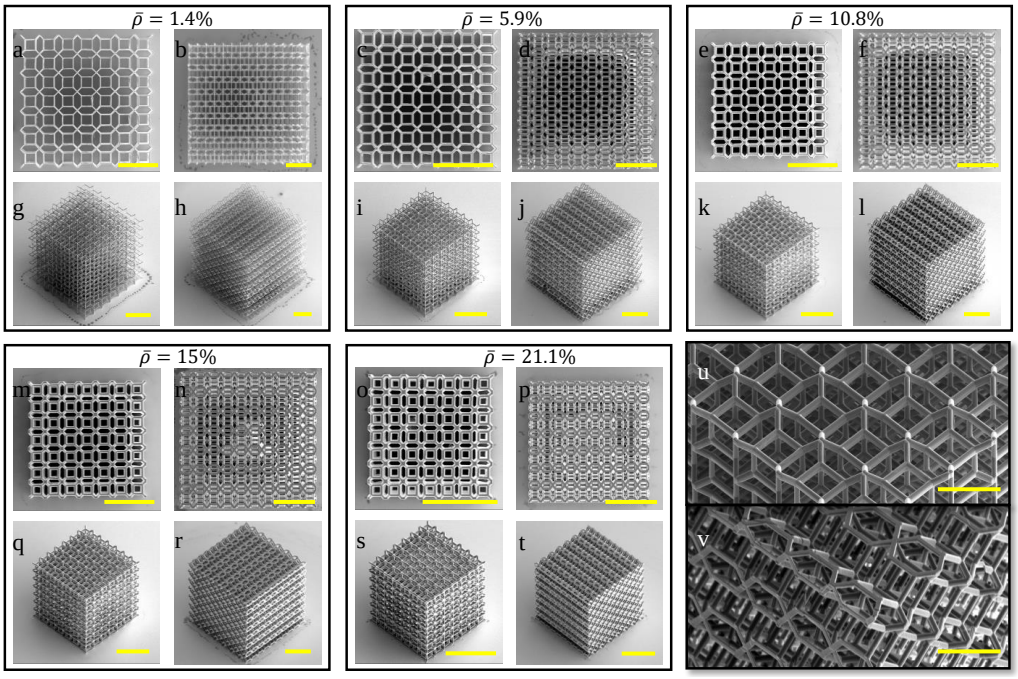

Figure 11: Scanning electron micrographs of BCC-SC truss micro-lattice samples fabricated via direct laser writing technology. (a–f) and (m–p) show top views of alternating [100] and [110] BCC-SC truss-lattice samples with varying relative density $\bar{\rho}$. (g-l) and (q-t) show isometric views of the same samples. (u) and (v) are close-up views of the samples with $\bar{\rho}$ = 5.9%. Scale bar lengths are (a–t) 300 μm and (u-v) 100 μm.

lower to upper boundaries in a layer by layer fashion. Compared with other stretching dominated lattices or buckling structures, the amplitude of oscillations are obviously smaller. This indicates that the post-collapse behavior should be stable and that the sightly buckling mode originates from the low resilience of thin struts to imperfections and flaws.

For relative density $\bar{\rho} = 5.9\%$, the buckling behavior of structures with ultra-low strut aspect ratio D/L is suppressed, and the deformation becomes uniform. The [100] sample exhibits an initially increasing elastic behavior followed by a weakly increasing elastic-plastic response (Figure 12b). The following plateauing behavior continues until the engineering strain reaches 0.25. During this process, the BCC-SC micro-lattice appears to possess a similar but enhanced bending-dominated mechanical behavior compared to the BCC lattice (see supporting material). This may be attributed to the facts that rotational micro-components allow for large steady deformations and that supporting micro-components provide additional structure stiffness and strength. Compared with other lightweight stretching-dominated truss lattices, such as the octet truss lattice [37] and other hybrid lattices [23], the stable post-collapse response makes the BCC-SC lattice more suitable for energy absorption. When the applied strain is larger than 0.25, rotational components contact each other and rotational degrees of freedom disappear. As a result, vertical struts have to support more bending moment, and are therefore very sensitive to shearing forces and flaws. When the compressive loading direction is not absolutely vertical, the shearing force introduced by friction between the loading stage and the sample results in uneven

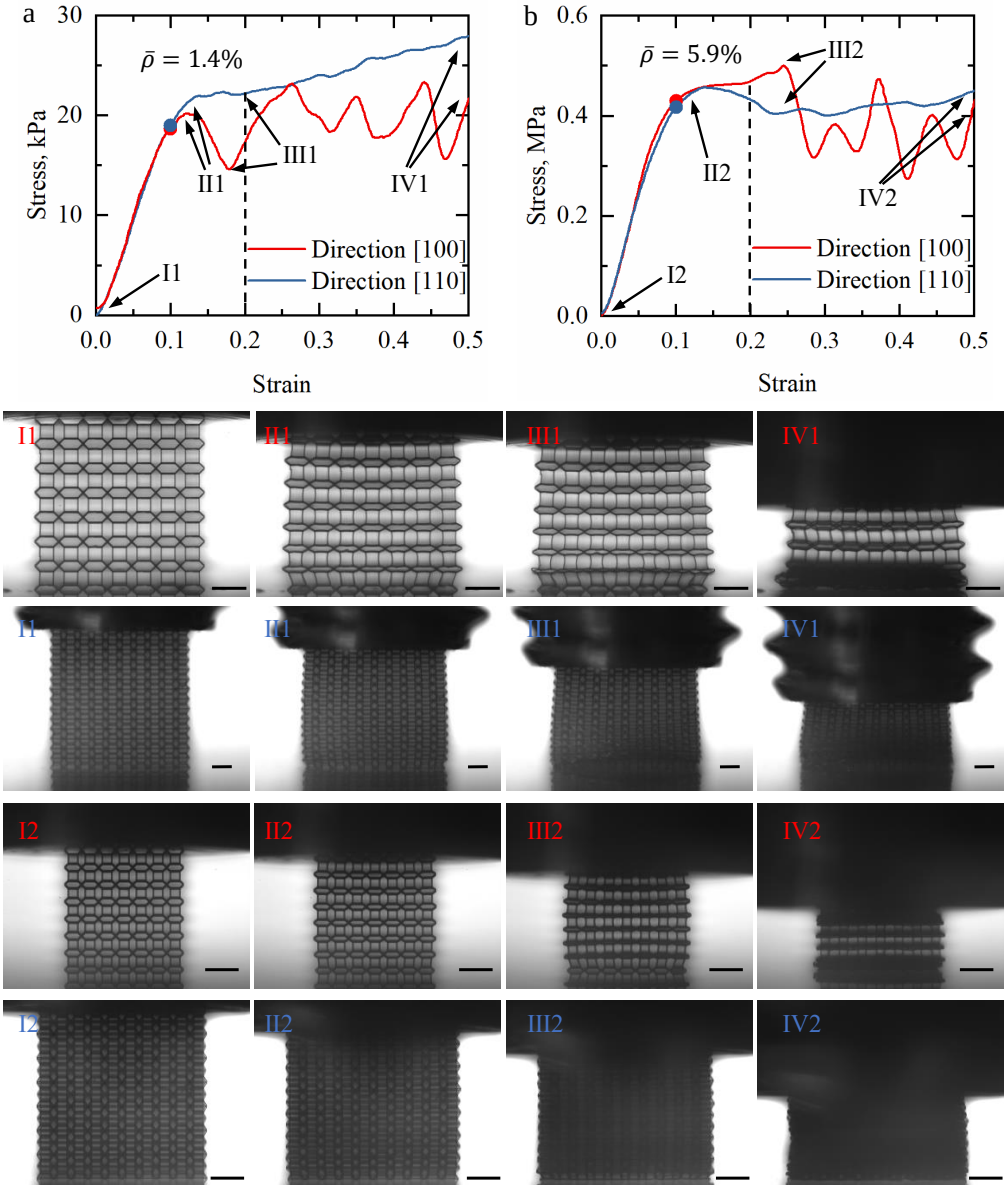

Figure 12: Compression experiments with BCC-SC micro-lattice samples fabricated by two-photon polymerization along directions [100] and [110]. (a) Nonlinear mechanical response and corresponding frames acquired during compression tests on samples with a relative density of 1.4%. Frames I to IV show the initial, collapse deformation, global unstably or steady deformation, and large compression up to maximum applied strain. (b) Nonlinear mechanical response and corresponding frames acquired during compression tests on samples with a relative density of 5.9%. Frames I to IV show the initial, collapse deformation, inelastic buckling, and large compression up to maximum applied strain. All scale bars are 200 μm long. The dotted line at 20% strain marks the upper limit of available numerical simulation data.

deformations. Hence, the mechanical behavior changes from a stable and increasing mode to an unstable and slightly oscillating mode.

The compressive response of samples with relative density $\bar{\rho}$ = 10.8% and 15% show trends similar to those at 5.9% relative density and their collapsing modes are similar. As the relative density increases, the unstable mechanical behavior at large strain gradually reduces. When the relative density is larger than 21.1%, oscillation modes disappear and the mechanical behavior is enhanced.

In contrast to [100] samples, all [110] samples exhibit almost the same elastic and elastic-plastic responses when the applied strain is less than 0.2. The following nonlinear response also appears to be more stable and to be slightly decreasing, at least for samples with relative density larger than 1.4%. Their stable behavior may be explained from the fact that [110] samples contain twice more rotational elements (i.e., inclined struts) compared to [100] samples, which provides enough rotational degrees of freedom to achieve stability. The decreasing response may be caused by brittle fracture of vertical struts (supporting elements) during fabrication (see Figure 11v) and by the smaller number of vertical struts.

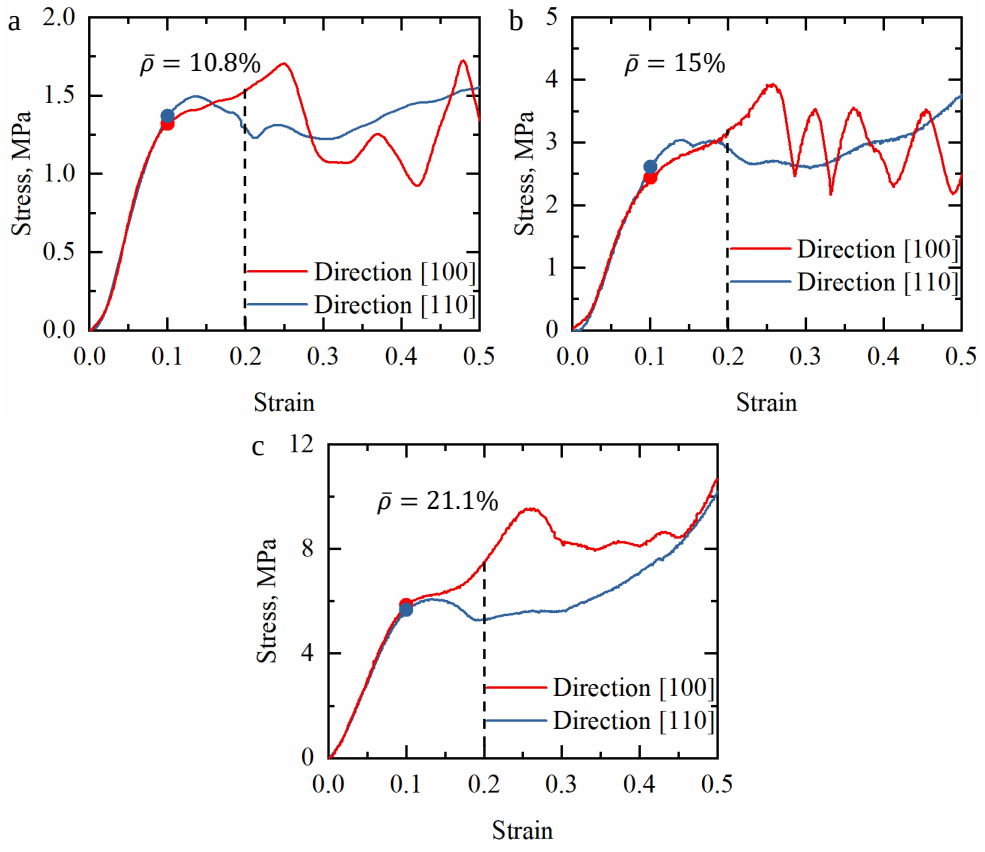

Figure 13: (a-c) Stress-strain curves are shown for samples with higher relative densities. The dotted line at 20% strain marks the upper limit of available numerical simulation data.

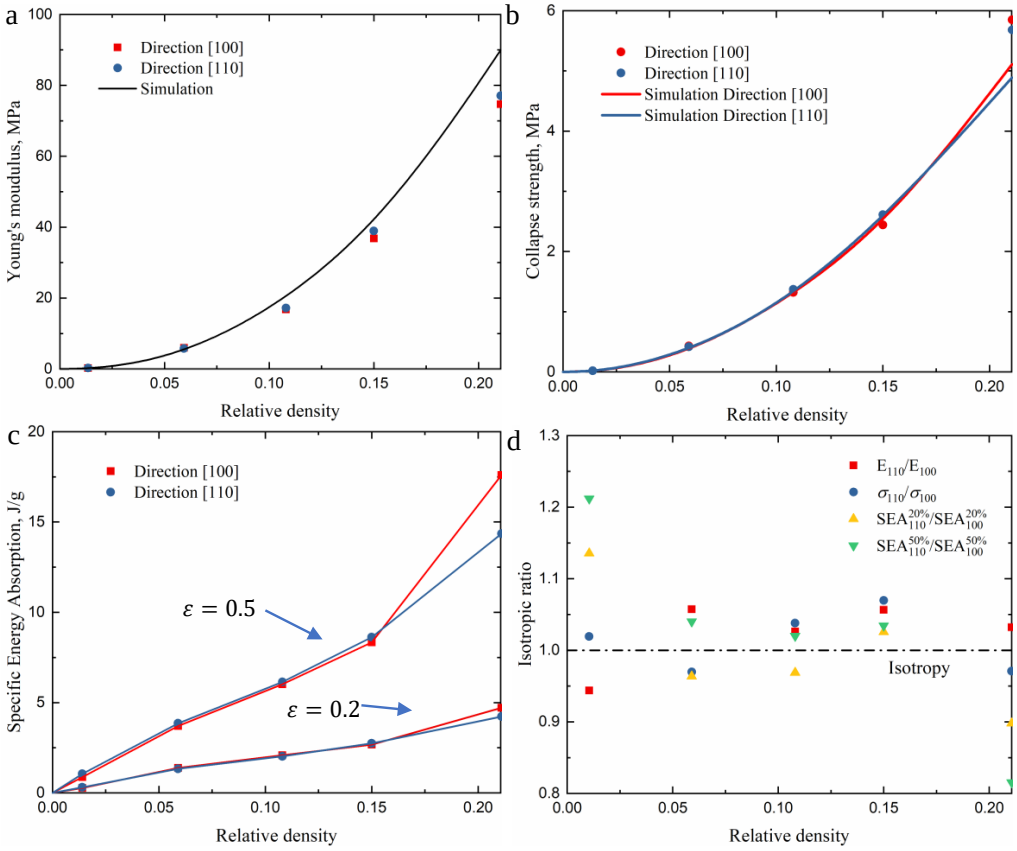

Figure 14: Mechanical data for samples measured during compression tests. (a) Young's modulus, (b) collapse strength, and (c) specific energy absorption are plotted against relative density for all tested samples. (d) Variations of isotropic ratios as a function of relative density demonstrate almost isotropic nonlinear mechanical response.

The experimental Young's modulus and collapse strength of all samples are found to be in good agreement with numerical simulation and analytical results (See Figure 14). Their elastic isotropy is confirmed by the fact that experimental data are close to the ideal linear isotropic ratio of 1 (See Figure 14d). Regarding nonlinear isotropy, more sample orientations would be necessary for a full characterization. The trends in the experimental results, however, are in line with simulations from the point of view of SEA. For all the relative densities considered, the deformation criterion, the failure mode and the nonlinear response of [100] samples are found to be similar to those of [110] samples when the applied strain is smaller than 0.2. The extreme values of the nonlinear isotropy ratios are about 1.13 and 0.9, and are found with samples with relative densities 0.01 and 0.2. For other relative densities, the nonlinear isotropic ratios are found to be close to 1.

Additional experimental studies performed with the BCC lattice and gathered in the supporting material show that the BCC-SC lattice always possesses a relative strength about 1.6 times as large and a normalized SEA about 1.64 times as large as that of the BCC lattice (see Figures S3). To further support this point, Figure 15 presents an Ashby plot of $SEA_{20\%}$ against Young's modu-

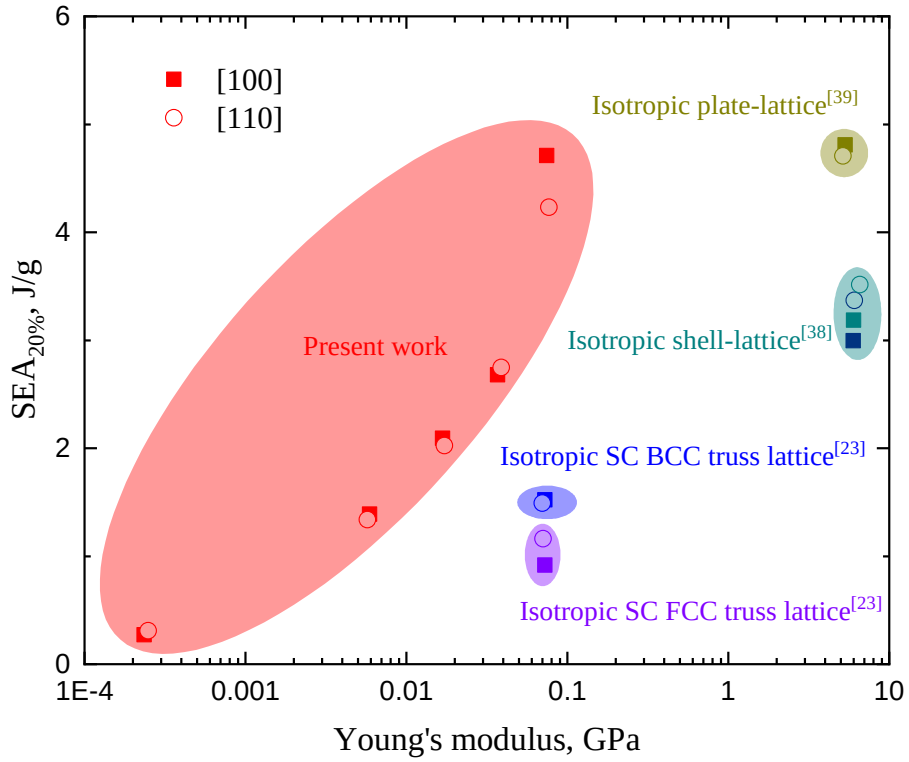

Figure 15: Ashby plot showing the $SEA_{20\%}$ versus the Young's modulus for various lightweight lattice structure samples, including isotropic BCC-SC lattices in this paper, isotropic SC BCC truss lattices [23], isotropic SC FCC truss lattices [23], isotropic shell lattices [38], and isotropic plate lattices [39].

lus, comparing the mechanical properties of lightweight lattice materials, including the proposed isotropic BCC-SC lattices, isotropic SC BCC truss lattices [23], isotropic SC FCC truss lattices [23], isotropic shell lattices [38], and isotropic plate lattices [39]. In comparison, the proposed BCC-SC truss lattices achieve a similar SEA with a much lower Young's modulus. It is noteworthy that the BCC-SC lattice with a relative density of 0.01 has a Poisson's ratio that almost attains the upper bound, 0.5, for isotropic materials (see supporting material). The BCC-SC lattice exhibits a fairly large ratio of bulk modulus to shear modulus, $K/G = 90.6$, which makes it potentially interesting for transformation elastodynamics. These mechanical behaviors make the proposed lattice a promising candidate for applications to static compression and dynamic shock.

5. Conclusion

In this paper, we have introduced a class of isotropic bending dominated truss lattice materials, formed by replacing the central connecting node of the body-centered cubic (BCC) truss lattice with a simple cubic (SC) truss lattice element, and we have examined its properties for energy absorption. The effective mechanical properties have been investigated both theoretically

and numerically. Results show that the designed metamaterials exhibit not only isotropic stiffness, but also nearly isotropic inelastic large deformation response. A series of samples with different relative densities were printed using two-photon polymerization in two different crystallographic directions, [100] and [110]. Uniaxial compression tests confirm that the BCC-SC lattice possesses nearly isotropic inelastic large deformation response together with isotropic elastic properties. The designed metamaterial is thus a noteworthy alternative for load bearing, energy absorption, and transformation acoustics.

Declaration of Competing Interest

The authors declare that they have no known competing financial interests or personal relationships that could have appeared to influence the work reported in this paper.

CRediT authorship contribution statement

X.C. designed research; X.C., Q.J., G.U., X.Y. and J.M. performed research; X.C. analyzed data; X.C., H.T., V.L. and M.K. wrote the paper.

Acknowledgements

J.M., M.K. and V.L. acknowledge support by the EIPHI Graduate School (contract ANR-17-EURE-0002) and the French Investissements d'Avenir program, project ISITE–BFC (contract ANR-15-IDEX-03). This work was partly supported by the french RENATECH network and its FEMTO-ST technological facility.

References

[1] C. Coulais, A. Sabbadini, F. Vink, M. van Hecke, Multi-step self-guided pathways for shape-changing metamaterials, Nature 561 (7724) (2018) 512–515.

[2] B. Florijn, C. Coulais, M. van Hecke, Programmable mechanical metamaterials, Physical Review Letters 113 (17) (2014) 175503.

[3] G. W. Milton, A. V. Cherkaev, Which elasticity tensors are realizable?, Journal of Engineering Materials and Technology 117 (4) (1995) 483–493.

[4] G. W. Milton, Complete characterization of the macroscopic deformations of periodic unimode metamaterials of rigid bars and pivots, Journal of the Mechanics and Physics of Solids 61 (7) (2013) 1543–1560.

[5] T. Frenzel, J. Köpfler, E. Jung, M. Kadic, M. Wegener, Ultrasound experiments on acoustical activity in chiral mechanical metamaterials, Nature Communications 10 (1) (2019) 1–6.

[6] T. Frenzel, M. Kadic, M. Wegener, Three-dimensional mechanical metamaterials with a twist, Science 358 (6366) (2017) 1072–1074.

[7] T. Bückmann, N. Stenger, M. Kadic, J. Kaschke, A. Frölich, T. Kennerknecht, C. Eberl, M. Thiel, M. Wegener, Tailored 3d mechanical metamaterials made by dip-in direct-laser-writing optical lithography, Advanced Materials 24 (20) (2012) 2710–2714.

[8] T. Bückmann, R. Schittny, M. Thiel, M. Kadic, G. W. Milton, M. Wegener, On three-dimensional dilational elastic metamaterials, New Journal of Physics 16 (3) (2014) 033032.

[9] X. Chen, J. Moughames, Q. Ji, J. A. I. Martínez, H. Tan, S. Adrar, N. Laforge, J.-M. Cote, S. Euphrasie, G. Ulliac, et al., Optimal isotropic, reusable truss lattice material with near-zero poisson's ratio, arXiv preprint arXiv:2003.07973 (2020).

[10] T. Frenzel, C. Findeisen, M. Kadic, P. Gumbsch, M. Wegener, Tailored buckling microlattices as reusable lightweight shock absorbers, Advanced Materials 28 (28) (2016) 5865–5870.

[11] S. Zhu, X. Tan, B. Wang, S. Chen, J. Hu, L. Ma, L. Wu, Bio-inspired multistable metamaterials with reusable large deformation and ultra-high mechanical performance, Extreme Mechanics Letters 32 (2019) 100548.

[12] X. Chen, Q. Ji, J. Wei, H. Tan, J. Yu, P. Zhang, V. Laude, M. Kadic, Light-weight shell-lattice metamaterials for mechanical shock absorption, International Journal of Mechanical Sciences 169 (2020) 105288.
[13] S. C. Han, J. W. Lee, K. Kang, A new type of low density material: Shellular, Advanced Materials 27 (37) (2015) 5506–5511.
[14] S. Zhu, J. Hu, X. Tan, B. Wang, S. Chen, L. Ma, Mechanics of sandwich panels with a buckling-dominated lattice core: The effects of the initial rod curvatures, Composite Structures 251 (2020) 112669.
[15] J. Berger, H. Wadley, R. McMeeking, Mechanical metamaterials at the theoretical limit of isotropic elastic stiffness, Nature 543 (7646) (2017) 533–537.
[16] H. Yang, L. Ma, 1d to 3d multi-stable architected materials with zero poisson's ratio and controllable thermal expansion, Materials & Design 188 (2020) 108430.
[17] X. Chen, H. Tan, An effective length model for octet lattice, International Journal of Mechanical Sciences 140 (2018) 279–287.
[18] T. George, V. Deshpande, H. Wadley, Hybrid carbon fiber composite lattice truss structures, Composites Part A: Applied Science and Manufacturing 65 (2014) 135–147.
[19] D. Jang, L. R. Meza, F. Greer, J. R. Greer, Fabrication and deformation of three-dimensional hollow ceramic nanostructures, Nature Materials 12 (10) (2013) 893–898.
[20] X. Zheng, H. Lee, T. H. Weisgraber, M. Shusteff, J. DeOtte, E. B. Duoss, J. D. Kuntz, M. M. Biener, Q. Ge, J. A. Jackson, et al., Ultralight, ultrastiff mechanical metamaterials, Science 344 (6190) (2014) 1373–1377.
[21] G. Gurtner, M. Durand, Stiffest elastic networks, Proceedings of the Royal Society A: Mathematical, Physical and Engineering Sciences 470 (2164) (2014) 20130611.
[22] T. Tancogne-Dejean, D. Mohr, Elastically-isotropic elementary cubic lattices composed of tailored hollow beams, Extreme Mechanics Letters 22 (2018) 13–18.
[23] T. Tancogne-Dejean, D. Mohr, Elastically-isotropic truss lattice materials of reduced plastic anisotropy, International Journal of Solids and Structures 138 (2018) 24–39.
[24] C. Bonatti, D. Mohr, Mechanical performance of additively-manufactured anisotropic and isotropic smooth shell-lattice materials: Simulations & experiments, Journal of the Mechanics and Physics of Solids 122 (2019) 1–26.
[25] R. Christensen, Mechanics of low density materials, Journal of the Mechanics and Physics of Solids 34 (6) (1986) 563–578.
[26] T. Tancogne-Dejean, M. Diamantopoulou, M. B. Gorji, C. Bonatti, D. Mohr, 3d plate-lattices: An emerging class of low-density metamaterial exhibiting optimal isotropic stiffness, Advanced Materials 30 (45) (2018) 1803334.
[27] C. Crook, J. Bauer, A. Guell Izard, C. Santos de Oliveira, J. Martins de Souza e Silva, J. B. Berger, L. Valdevit, Plate-nanolattices at the theoretical limit of stiffness and strength, Nature Communications 11 (1) (2020) 1–11.
[28] Y. Wang, O. Sigmund, Quasiperiodic mechanical metamaterials with extreme isotropic stiffness, Extreme Mechanics Letters 34 (2020) 100596.
[29] V. Deshpande, M. Ashby, N. Fleck, Foam topology: bending versus stretching dominated architectures, Acta Materialia 49 (6) (2001) 1035–1040.
[30] K. Ushijima, W. Cantwell, R. Mines, S. Tsopanos, M. Smith, An investigation into the compressive properties of stainless steel micro-lattice structures, Journal of Sandwich Structures & Materials 13 (3) (2011) 303–329.
[31] R. Gümrük, R. Mines, Compressive behaviour of stainless steel micro-lattice structures, International Journal of Mechanical Sciences 68 (2013) 125–139.
[32] T. Tancogne-Dejean, D. Mohr, Stiffness and specific energy absorption of additively-manufactured metallic bcc metamaterials composed of tapered beams, International Journal of Mechanical Sciences 141 (2018) 101–116.
[33] J. Hutchinson, Shear coefficients for timoshenko beam theory, J. Appl. Mech. 68 (1) (2001) 87–92.
[34] M. A. Meyers, K. K. Chawla, Mechanical behavior of materials, Cambridge university press, 2008.
[35] S. Li, A. Wongsto, Unit cells for micromechanical analyses of particle-reinforced composites, Mechanics of Materials 36 (7) (2004) 543–572.
[36] S. Suwas, R. K. Ray, Crystallographic texture of materials, Springer, 2014.
[37] T. Tancogne-Dejean, A. B. Spierings, D. Mohr, Additively-manufactured metallic micro-lattice materials for high specific energy absorption under static and dynamic loading, Acta Materialia 116 (2016) 14–28.
[38] Q. Ma, L. Zhang, J. Ding, S. Qu, J. Fu, M. Zhou, M. W. Fu, X. Song, M. Y. Wang, Elastically-isotropic open-cell minimal surface shell lattices with superior stiffness via variable thickness design, Additive Manufacturing 47 (2021) 102293.
[39] S. Duan, W. Wen, D. Fang, Additively-manufactured anisotropic and isotropic 3d plate-lattice materials for enhanced mechanical performance: Simulations & experiments, Acta Materialia 199 (2020) 397–412.